Journal of Magnetic Resonance **148,** 88–94 (2001)
doi:10.1006/jmre.2000.2223, available online at http://www.idealibrary.com on IDEAL®

HMSC: Simultaneously Detected Heteronuclear Shift Correlation through Multiple and Single Bonds[1]

Rémy Burger, Christian Schorn, and Peter Bigler[2]

Department of Chemistry and Biochemistry, University of Berne, Freiestrasse 3, CH-3012 Bern, Switzerland

Received May 30, 2000; revised August 29, 2000

A new 2D pulse sequence HMSC (heteronuclear multiple-bond and single-bond coupling connectivities) for the simultaneous detection of long-range and one-bond heteronuclear connectivities is proposed which allows the two types of responses to be separated and the corresponding $^{n}J_{CH}$ and $^{1}J_{CH}$ connectivity maps to be calculated. $^{n}J_{CH}$ coherences are selectively labeled in the course of the pulse sequence, the correspondingly acquired data are separately stored, and a simple add/subtract procedure is applied to disentangle and edit $^{n}J_{CH}$ and $^{1}J_{CH}$ responses prior to final data processing. Unlike standard methods, which are designed to measure one single type of heteronuclear spin–spin interactions and to efficiently suppress the other, both $^{n}J_{CH}$ and $^{1}J_{CH}$ are measured simultaneously in a single experiment with the HMSC pulse sequence. Compared to the common strategy with two standard experiments applied one after the other, e.g., HMBC and HMQC, valuable measuring time may be saved with this single experiment approach. The efficiency of the new pulse sequence and the quality of the corresponding spectra are demonstrated using strychnine. Features such as sensitivity, lineshapes, and the suppression of $^{1}J_{CH}$ residual peaks in the final $^{n}J_{CH}$ subspectra are investigated and compared with the corresponding results obtained with standard methods. The attractive and unique single experiment approach, its high efficiency, and its easy experimental setup together with straightforward data processing make HMSC a valuable experimental alternative for the today's more time-consuming "two-step" practice and makes it suitable for standard routine applications. © 2001 Academic Press

Key Words: **long-range heteronuclear shift correlation; one-bond heteronuclear shift correlation; HMBC; HMQC; HMSC.**

INTRODUCTION

Multidimensional heteronuclear shift correlation between directly and remotely coupled nuclei is probably the most powerful tool of high-resolution NMR spectroscopy. Whereas $^{1}J_{CH}$ connectivities and coupling constants are mainly used to check and establish signal assignments of protons bearing carbons and to extract information on functional groups and carbon hybridization degrees, respectively, $^{n}J_{CH}$ connectivities and coupling constants are probably much more valuable for establishing molecular structures. "Long-range" connectivities allow carbon signal assignments, including quaternary carbons, to be completed. Corresponding coupling constants allow structural fragments to be connected unequivocally and complex stereochemical problems to be solved in a straightforward way. Reliable ^{13}C signal assignments based on $^{1}J_{CH}$ connectivities and assigned ^{1}H signals are a prerequisite, however, for the interpretation of $^{n}J_{CH}$ correlation spectra. Consequently, information on both types of coupling interactions is usually needed for unequivocal conclusions with more demanding structural problems. Today's heteronuclear shift correlation experiments are dedicated to detecting either type of coupling interaction while destructively rejecting the other. Therefore, at least two experiments for detecting both types of heteronuclear connectivities must be performed. To the best of our knowledge no methods for simultaneous detection of $^{1}J_{CH}$ and $^{n}J_{CH}$ connectivities exist, which allows the two types of responses to be separated and the corresponding subspectra to be calculated.

The main requirements for such a method may be summarized as follows: Equal or at least similar sensitivities especially for measuring $^{n}J_{CH}$ connectivities compared to today's state-of-the-art experimental alternatives; powerful filters for rejecting unwanted $^{1}J_{CH}$ signals in the final $^{n}J_{CH}$ subspectrum ("$^{n}J_{CH}$ low-pass" filter) and vice versa for rejecting unwanted $^{n}J_{CH}$ signals in the final $^{1}J_{CH}$ subspectrum ("$^{1}J_{CH}$ high-pass" filter); unlimited applicability with respect to the range of $^{n}J_{CH}$ and $^{1}J_{CH}$ coupling constants, the corresponding multiplicities, and the degree of complexity in the ^{1}H spectrum; easy experimental setup for routine applications.

The starting point for our efforts was the prominent HMBC (*1*) pulse sequence and its modern variants. A breakthrough for the heteronuclear multiple-bond correlation (heteronuclear multiple-bond correlation (HMBC)). (HMBC) experiment compared to former pulse sequences was ^{1}H detection and the introduction of pulsed field gradients (*2*, *3*). Modifications of the HMBC experiment with an additional delay for refocusing long-range couplings with additional ^{13}C broadband decoupling have been proposed (*4*), and phase-sensitive experiments with single-quantum evolution in $t1$ were developed (*5*, *6*) as well as experiments with a constant time evolution period for

[1] First presented at the 15th European Experimental NMR Conference, Leipzig, Germany, June 2000.

[2] To whom correspondence should be addressed.

1090-7807/01 $35.00

suppressing J-modulation due to ^{1}H–^{1}H couplings in F1 (*7*). Despite its high detection sensitivity, the gradient-enhanced HMBC experiment suffers from a poor low-pass filter quality with a breakthrough of unwanted $^1J_{CH}$ signals. Furthermore, the experiment may not be adjusted to sample the wide range of $^nJ_{CH}$ coupling constants (1–25 Hz) in a uniform manner and important cross peaks may be rather weak or may even be lost in a HMBC spectrum.

Modified variants to improve low-pass filter efficiency with the implementation of an additional BIRD-relaxation filter (*8*) or an additional TANGO filter (*9*) have been developed. Efforts for uniform sampling of long-range couplings have been undertaken and corresponding experiments have been proposed, e.g., a 3D HMBC (*10*) with the third dimension used for "scanning" the whole range of $^nJ_{CH}$ couplings. Among these developments, the ACCORDION-HMBC (*11*) experiment is probably the most popular and promising since it not only suppresses $^1J_{CH}$ signals more efficiently, but also samples in a systematic fashion and in a single experiment a potentially wide range of long-range couplings exploiting the ACCORDION principle (*12*). It is designed as a "refocused" variant for optional ^{13}C broadband decoupling during data acquisition. However, a few minor drawbacks remain with this experiment: There is a general loss of sensitivity compared to the basic HMBC and J_{HH} modulation in $t1$ introduced with the ACCORDION principle, which gives rise to additional cross peaks in F1. These additional peaks may prove the authenticity of correlations but may also make spectral analysis more difficult (*13*). Efforts for suppressing these undesirable ACCORDION "artifacts" taking advantage of a "constant time variable delay" pulse sequence element have been undertaken and correspondingly improved pulse sequences, IMPEACH-MBC (*14*) and CIGAR-HMBC (*15*), have very recently been proposed. Furthermore, FID shapes are obtained with the ACCORD-HMBC, which are unsuitable for simultaneously obtaining narrow lineshapes and maximum sensitivity with magnitude mode calculation.

In this work we present a simple new 2D pulse sequence HMSC (heteronuclear shift correlation through multiple and single bonds) for the simultaneous detection of $^nJ_{CH}$ and $^1J_{CH}$ coupling interactions. The pulse sequence was developed and optimized taking advantage of the powerful simulation tool NMRSIM (*16*), which allowed experimental parameters such as delays, pulse lengths, or pulse power for a given spin system to be varied systematically and its influence on sensitivity and filter efficiency to be studied in detail. Spectra obtained with strychnine are compared with the spectra correspondingly obtained with the HMBC, the ACCORD-HMBC, and the HMQC experiment.

RESULTS AND DISCUSSION

Figure 1 shows the HMSC pulse sequence developed for the simultaneous detection of $^nJ_{CH}$ and $^1J_{CH}$ coupling interactions, encompassing high sensitivity, efficient filtering for both kinds of coupling interactions, and attractive lineshapes with magnitude mode spectra.

The HMSC experiment starts with a 90° ^{1}H pulse, followed by a BIRD$_y$ element (*17*), incorporated in the middle of the delay for the evolution of long-range coupling interactions. The corresponding delays $D2 = (2 \cdot {}^1J_{CH})^{-1}$ and $D3 = (4 \cdot {}^nJ_{CH})^{-1}$ are adjusted for one-bond and long-range couplings, respectively. Neglecting homonuclear couplings at this stage, transverse ^{1}H magnetization generated by the initial 90° ^{1}H pulse evolves in the course of the BIRD$_y$ element either and exclusively under the influence of long-range couplings for $^nJ_{CH}$ coupled protons ($^nI_y \Rightarrow 2{}^nI_xS_z$) or under the influence of ^{1}H chemical shifts for $^1J_{CH}$ coupled protons ($^1I_y \Rightarrow {}^1I_y, {}^1I_x$) as described in detail elsewhere (*17*). This allows coherence of $^nJ_{CH}$ coupled protons to be labeled selectively at this stage of the pulse sequence with a ^{13}C pulse adjusted either to 180 or to 0° ($2{}^nI_xS_z \Rightarrow \pm 2{}^nI_xS_z$), whereas coherence of $^1J_{CH}$ coupled protons is not affected by the ^{13}C pulse ($^1I_y, {}^1I_x \Rightarrow {}^1I_y, {}^1I_x$). The best results in view of eventually incorrectly set ^{13}C pulse lengths are obtained with 90°_x–180°_y–90°_x and 90°_x–180°_{-x}–90°_x ^{13}C composite pulses, respectively. In contrast to the in-phase $^1J_{CH}$ coherence, which evolves under the influence of direct couplings and proton chemical shifts into antiphase coherence ($2{}^1I_xS_z$, $2{}^1I_yS_z$) in the subsequent $D2$ delay, almost no additional coupling evolution occurs for $^nJ_{CH}$ coherence. The next 90° ^{13}C pulse transforms $^nJ_{CH}$ and $^1J_{CH}$ antiphase components into multiquantum coherences, which evolve in $t1$ exclusively under the influence of ^{13}C chemical shifts. $^nJ_{CH}$ and $^1J_{CH}$ multiquantum coherences are transformed back into detectable proton single-quantum coherences by the last 90° ^{13}C pulse and are detected simultaneously with no ^{13}C broadband decoupling during data acquisition.

As with the basic HMBC experiment, homonuclear coupling evolves throughout. J-Modulation due to ^{1}H–^{1}H coupling evolution during the $t1$ period causes line broadening of the ^{13}C signals in the F1 dimension (*7*).

To preserve and exploit the $^nJ_{CH}$ selective labeling of proton signals, achieved with the composite ^{13}C pulse for the subsequent separation of one-bond and "long-range" responses in two subspectra, FIDs are acquired in the so-called "interleaved mode." For each $t1$ increment, two FIDs with the phase $\varphi 2$ (Fig. 1) set as y or $-x$, respectively, are acquired and stored separately. In the first step of data processing, each $t1$ pair is split and two intermediate 2D matrices are generated from the original 2D data matrix. To obtain the final two spectra with the $^1J_{CH}$ and $^nJ_{CH}$ responses disentangled from each other, these two intermediate 2D matrices are added to and subtracted from each other, respectively (spectral editing). Data are processed in the same way as the HMBC data and the corresponding 2D magnitude mode (in F1) spectra are then calculated (for details see the legends to Figs. 2 and 3).

The high filter efficiencies are due to the following: If the delay $D2 = (2 \cdot {}^1J_{CH})^{-1}$ is not optimally adjusted, $^1J_{CH}$

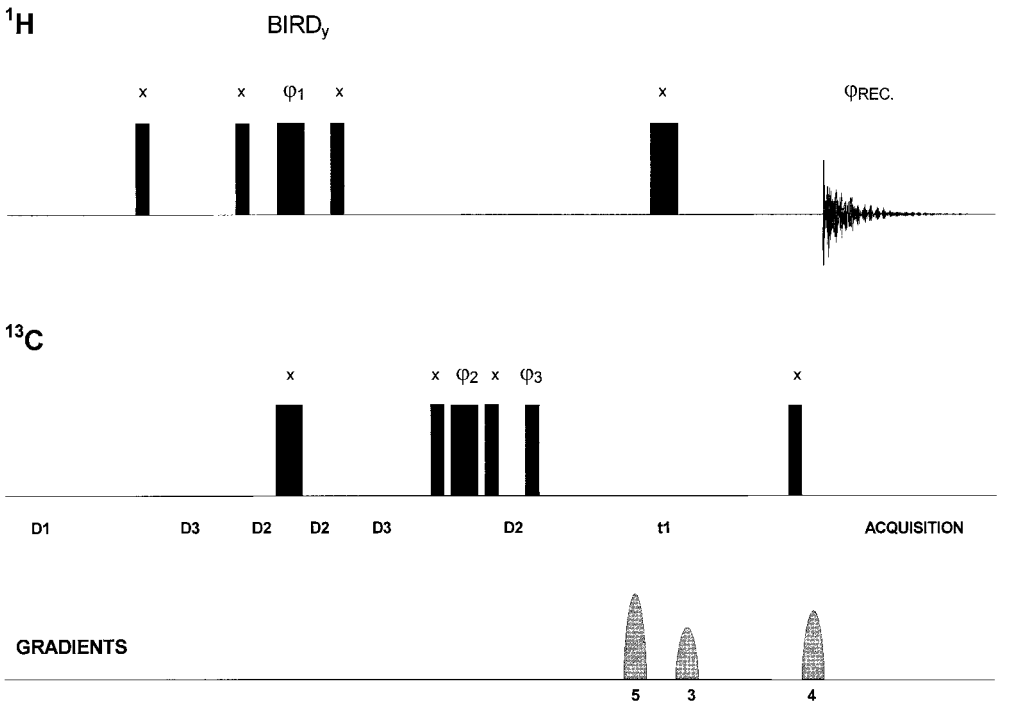

FIG. 1. HMSC pulse sequence for the detection of $^{n}J_{CH}$ and $^{1}J_{CH}$ connectivities. Thin and thick bars represent 90 and 180° pulses, respectively. The first ^{13}C 180° pulse is replaced by a 90°_{x}–180°_{y}–90°_{x} composite pulse. $D2$ is set to $(2 \cdot {}^{1}J_{CH})^{-1}$ and $D3$ is set to $(4 \cdot {}^{n}J_{CH})^{-1}$. For each $t1$ value two $t2$-FIDs with different phase settings $\varphi_2 = y, -x$ are acquired and separately stored ("interleaved" mode of detection). The residual phases in the experiment are cycled as follows: $\varphi_1 = y(-y)$; $\varphi_3 = x_2(-x)_2$; $\varphi_{REC} = x_2(-x)_2$. Using standard Bruker software the two $t1$ sets, differing in the sign of $^{n}J_{CH}$ proton signals, are disentangled and stored in two submatrices, which are either added to or subtracted from each other to calculate the final data matrices with the $^{1}J_{CH}$ and $^{n}J_{CH}$ responses separated (spectral editing). The Bruker DRX pulse program and the modified Bruker Splitser.AU programs for data processing (see legend to Fig. 2) are available from the authors upon request.

in-phase coherences evolve partially into $2^{1}I_{x}S_{z}$ and $2^{1}I_{y}S_{z}$ antiphase coherences, respectively, during the BIRD$_y$ pulse sequence element. The ^{13}C labeling pulse affects these $^{1}J_{CH}$ antiphase coherences in the same way as the $^{n}J_{CH}$ antiphase coherences ($2^{1}I_{x,y}S_{z} \Rightarrow \pm 2^{1}I_{x,y}S_{z}$), giving rise to $^{1}J_{CH}$ residual peaks in the final $^{n}J_{CH}$ spectrum. These peaks, however, are efficiently suppressed by the subsequent $D2$ delay. Most of the unwanted $^{1}J_{CH}$ antiphase coherences evolve back into in-phase coherence and are not transferred into multiquantum coherence by the 90° ^{13}C prior to the $t1$ period ($^{n}J_{CH}$ low-pass filter).

If, on the other hand, the delay $D3 = (4 \cdot {}^{n}J_{CH})^{-1}$ for the evolution of long-range couplings is not adjusted optimally, initial in-phase $^{n}J_{CH}$ coherences survive the BIRD$_y$ element and are not affected by the ^{13}C labeling pulse. Part of these in-phase coherences, however, evolves into antiphase coherences during the subsequent $D2$ delay and is transferred into multiquantum coherence, giving rise to residual $^{n}J_{CH}$ peaks in the final $^{1}J_{CH}$ subspectrum. Since D3 is adjusted to large $^{n}J_{CH}$ couplings, the unwanted in-phase terms predominantly originate from interactions with small couplings. Almost no evolution into antiphase coherence occurs for these terms during the short $D2$ delay, and consequently only spurious residual $^{n}J_{CH}$ peaks are observed in the final $^{1}J_{CH}$ spectrum ($^{1}J_{CH}$ high-pass filter).

To maintain the highest sensitivity and to achieve the best low-pass filter efficiency, the same phase cycle, slightly expanded for the phase of the 180° ^{1}H pulse in the BIRD element, as that proposed for the gradient enhanced HMBC experiment (*3*) was used. In addition to the ^{13}C labeling pulse (see before) and to compensate for incorrectly set ^{13}C pulse angles, the 180° ^{13}C pulse in the BIRD element was replaced by composite pulses. (90°_{x}–180°_{y}–90°_{x}) (*18*).

For measuring ^{13}C broadband decoupled spectra, $^{n}J_{CH}$ and $^{1}J_{CH}$ coherences must be refocused prior to data acquisition. This may be accomplished with two additional BIRD elements (BIRD$_y$ and BIRD$_x$) after the $t1$ period and with the phase cycle and gradient pulse settings adjusted accordingly. The HMSC sequence was tested on strychnine.

For comparison, spectra were acquired with the basic HMBC and HMQC (with/without refocusing) experiments and with the recently proposed ACCORD-HMBC experiment. Spectra were measured with and without ^{13}C GARP decoupling during acquisition for all refocused experiments and with the ACCORD option enabled and disabled for the ACCORD-HMBC experiment. In order to compare the results, experimental conditions were set as similar as possible and exactly the same measuring times were maintained with each experiment. Consequently, either the $^{1}J_{CH}$ or the $^{n}J_{CH}$ spectrum could be acquired within this preset measuring time with the HMQC

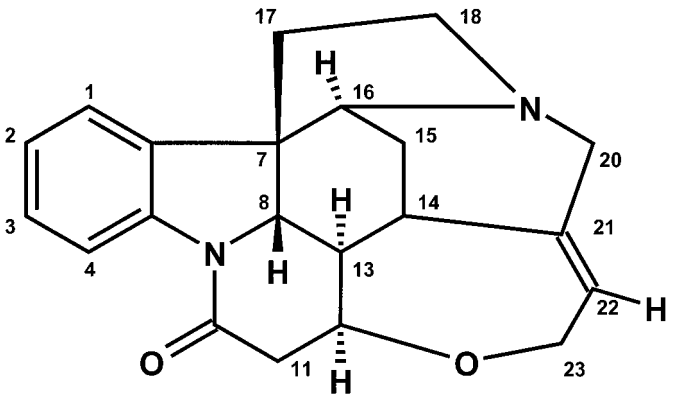

SCHEME 1

and the HMBC or ACCORD-HMBC experiments, respectively, whereas both types of spectra could be obtained with the HMSC experiment and adequate data processing.

Figure 2 shows expansions (aliphatic part) of the $^{n}J_{CH}$ (left) and the $^{1}J_{CH}$ (right) connectivity spectra of strychnine obtained with the HMSC experiment. The excellent discrimination between $^{n}J_{CH}$ and $^{1}J_{CH}$ cross peaks achieved with the HMSC experiment with no residual cross peaks of the other type left in the corresponding subspectra is obvious.

Figures 3 and 4 show representative rows of the corresponding 2D spectra with the $^{n}J_{CH}$ and $^{1}J_{CH}$ connectivities of carbons C-14 and C-23, respectively.

Concentrating on sensitivity and long-range interactions first, it follows from Fig. 3 that with the HMSC experiment, only minor sensitivity losses must be taken into account compared to the HMBC experiment. On the other hand, and irrespective of whether ^{13}C GARP decoupling is applied, a substantial gain in sensitivity compared to the ACCORD-HMBC experiment is obtained, which is most pronounced for weak cross peaks. The unwanted discrimination of weak cross peaks observed in the static ACCORD-HMBC spectra must be attributed to the additional delays. With the ACCORDION option enabled, this discrimination, but not the general decrease in sensitivity, may more or less be avoided. For cross peaks in the $^{1}J_{CH}$ HMSC subspectra (Fig. 4), a decrease in sensitivity of about 15% compared to the nondecoupled HMQC spectrum has been observed, most probably because of additional relaxation losses with the long $D3$ delays. A decrease in sensitivity of about 50% must be taken into account compared to the ^{13}C GARP decoupled HMQC spectrum. Signal intensities are nevertheless well above the intensities of most of the $^{n}J_{CH}$ cross peaks and their doublet structure may not severely complicate spectral analysis.

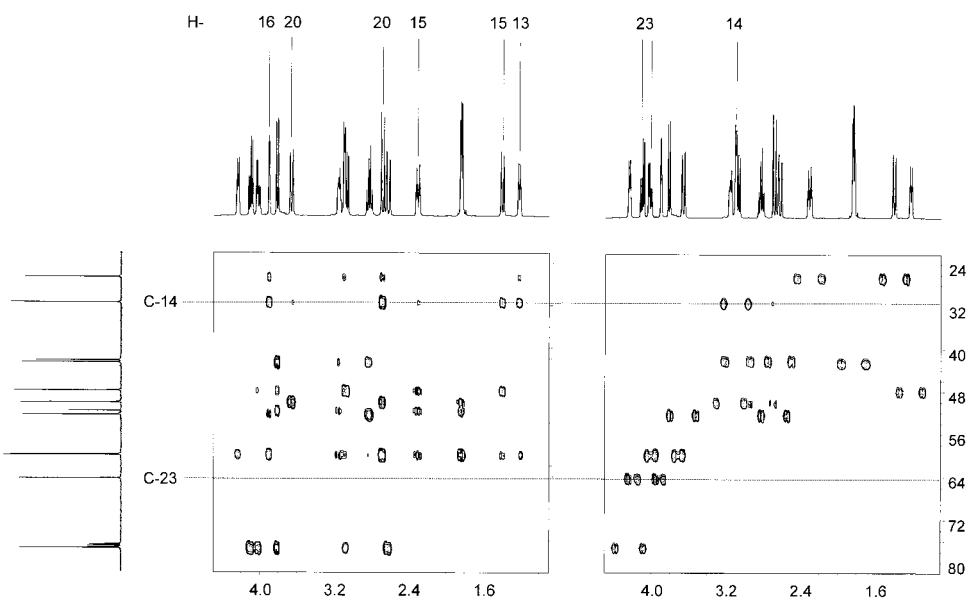

FIG. 2. $^{n}J_{CH}$ and $^{1}J_{CH}$ 2D spectra of strychnine (expansion of the aliphatic region) measured with the HMSC pulse sequence. A sample of 60 mg of strychnine in 200 μl $CDCl_3$ in a sealed 5-mm NMR tube (Wilmad) was used. The experiments were performed on a Bruker DRX-500 spectrometer operating at a proton resonance frequency of 500.13 MHz with a 5-mm inverse probehead (TBI) equipped with additional coils for z-gradients and with 90° pulse lengths of 6.9 and 15 μs for ^{1}H and ^{13}C, respectively. Delays $D1$, $D2$ ($2 \cdot {}^{1}J_{CH}^{-1}$), and $D3$ ($4 \cdot {}^{n}J_{CH}^{-1}$) were set as 2 s, 3.45 ms (optimized for $^{1}J_{CH} = 145$ Hz), and 25 ms (optimized for $^{n}J_{CH} = 10$ Hz), respectively. The delay for phase switching within the ^{13}C composite pulses was set to 5 μs. Each 2D spectrum was collected with ^{1}H and ^{13}C spectral widths of 5000 and 22637 Hz, respectively. Eight scans using 2048 data points in $t2$ were acquired for each 2×256 FID with the "interleaved" mode of detection. In the first step of data processing the original 2D data were split into two new data sets by using the slightly modified Splitser.AU (Bruker) program. Each of these two data sets was apodized with a 45° shifted sine square function and Fourier transformed in $t2$. To disentangle the responses of one-bond and long-range coupling interactions, these data sets were then added to and subtracted from each other. The final $^{1}J_{CH}$ and $^{n}J_{CH}$ subspectra were obtained after apodization with a nonshifted sine square function, zero filling to 512 points, and Fourier transformation in $t1$ and with magnitude mode calculation in F1. The same contour levels are used for both subspectra. Rows for C-14 and C-23 are indicated and the ^{1}H signals of corresponding cross peaks are assigned.

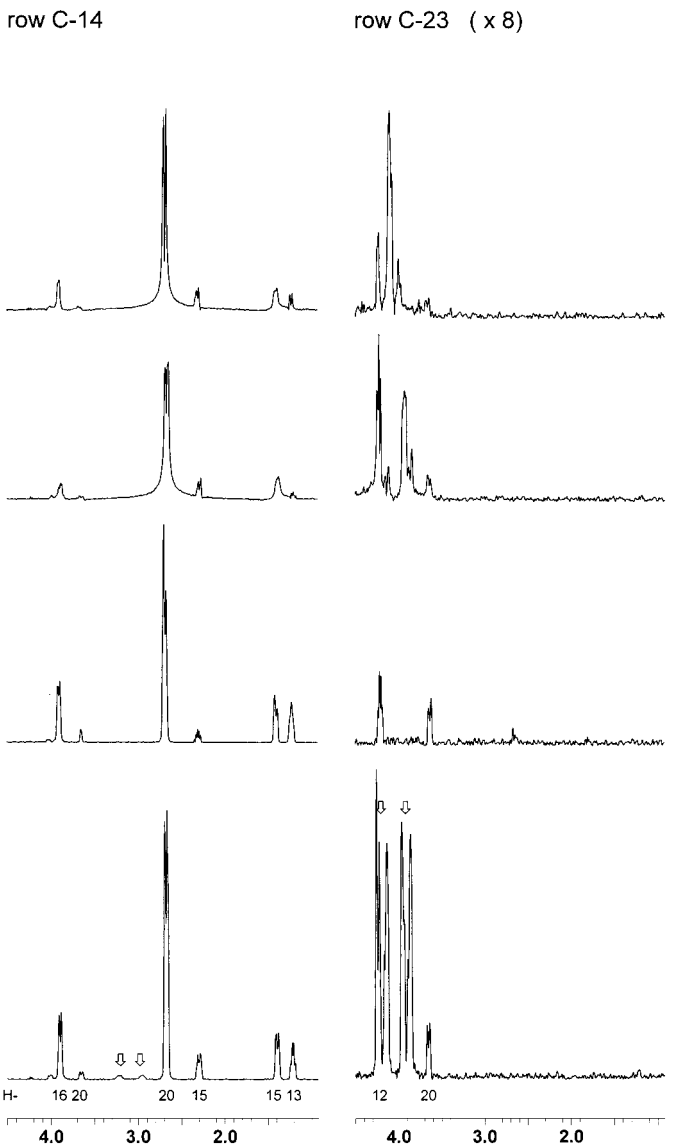

FIG. 3. Representative rows with the $^{n}J_{CH}$ connectivities of C-14 and C-23 demonstrating the sensitivities and lineshapes obtained with the HMBC, the HMSC, and the ACCORD-HMBC with and without ^{13}C GARP decoupling (from bottom to top) are shown. The same experimental parameters as those given for the HMSC experiment (see legend to Fig. 2) were used for the HMBC and the ACCORD-HMBC experiment with the exception of the $^{n}J_{CH}$ evolution delay ($2^{n}J_{CH}^{-1}$), which was set to 50 ms (optimized for $^{n}J_{CH} = 10$ Hz) and the $^{1}J_{CH}$ delays in the two low-pass filters of the ACCORD-HMBC experiment. Following the recommendations of the authors, different values were used for the two filters according to the formula $0.5 \cdot (^{1}J_{min/max} \pm 0.146(^{1}J_{max} - {}^{1}J_{min}))^{-1}$ with $J_{min} = 125$ Hz and $J_{max} = 165$ Hz as 3.82 and 3.14 ms, respectively. For the ACCORD-HMBC experiment, the ACCORDION option was disabled and a "static" delay was applied for direct comparison with the other "static" experiments. Eight sinusoidally shaped gradient pulses in the ratio 15:−10:−5:50:30:40:−5:5 were used for ACCORD-HMBC. Squared sinebell windows in $t2$ were shifted by 45 and 90° for HMBC/HMSC and ACCORD-HMBC, respectively, to achieve the best sensitivities (rather than the same narrow lines) with the differing FID shapes of these experiments. Data acquired with the HMSC experiment were processed as described in the legend to Fig. 2. An enhanced vertical scale was used for the row of C-23 showing very small long-range cross peaks. Note that for this carbon atom a weak $^{4}J_{CH}$ coupling to H-20 is visible. ^{1}H signals of corresponding long-range cross peaks are assigned. Residual $^{1}J_{CH}$ signals are indicated.

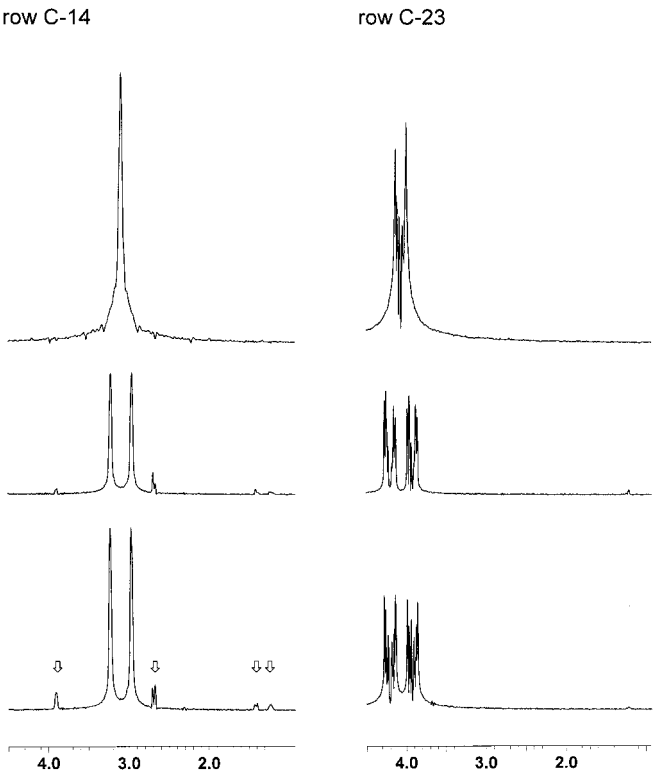

FIG. 4. Representative rows with the $^{1}J_{CH}$ connectivities C-23/H-$23_{a,b}$ and C-14/H-14 demonstrating the sensitivities and lineshapes obtained with the nonrefocused HMQC, the HMSC, and the refocused HMQC with ^{13}C GARP decoupling (from bottom to top) are shown. The same experimental parameters as those given for the HMSC experiment (see legend to Fig. 2) were correspondingly used for the HMQC experiment. Squared sinebell windows in $t2$ were shifted by 45 and 90° for the nonrefocused and the refocused experiments, respectively, to achieve the best sensitivities in each case. Data acquired with the HMSC experiment were processed as described in the legend to Fig. 2. Residual long-range cross peaks are indicated.

Concentrating on filter efficiencies next, excellent results are obtained for the more demanding $^{n}J_{CH}$ spectra with the HMSC experiment (Fig. 3). Extreme high $^{1}J_{CH}$ suppression degrees are of utmost importance and are a prerequisite for the reliable detection and recognition of very weak long-range couplings which are valuable for the connecting remote molecular fragments. Such cross peaks may otherwise be overseen, may be mistaken for, or may accidentally be hidden by residual $^{1}J_{CH}$ peaks. The row of C-23 (Fig. 3) in the HMBC spectrum shows that the residual $^{1}J_{CH}$ signals fully dominate and overlap with one of the weak "long-range" cross peaks. The high $^{1}J_{CH}$ suppression degrees obtained with the ACCORD-HMBC (with the ACCORD option enabled or not) are even surpassed with the HMSC experiment. Almost no residual $^{1}J_{CH}$ signals appear

in the row of C-23 and the weak long-range cross peaks, one of which originates from a $^4J_{CH}$ coupling, are clearly visible.

Suppression of $^nJ_{CH}$ cross peaks in HMSC $^1J_{CH}$ subspectra (Fig. 4) is less efficient as discussed before and weak residual long-range peaks are still visible. However, $^1J_{CH}$ High-pass filtering is less demanding since one-bond cross peaks clearly dominate and their doublet structure may easily be recognized.

Spectral lineshapes and sensitivity are also influenced by the FID shapes and data processing. With nonrefocused experiments (HMBC, HMSC), the individual $t2$ FID shapes are dominated by the low-frequency term $\sin 2\Pi^nJ_{CH} \cdot t2$ with a maximum at $t2 = (2^nJ_{CH})^{-1}$, usually close to the midpoint of the time domain signal. Attractive narrow signal lineshapes with no additional loss of sensitivity result in an adequate weighting, e.g., with a (Π/4) shifted sinebell function and subsequent magnitude calculation. With refocused variants (ACCORD-HMBC), on the other hand, antiphase coherence evolves into in-phase coherence prior to detection ($2I_xS_y \Rightarrow I_y$). The corresponding $t2$-FID shapes, dominated by the low-frequency term $\cos 2\Pi^nJ_{CH} \cdot t2$, decay steadily and are not ideal for subsequent magnitude calculation. Weighting optimized for narrow lineshapes, e.g., with an adequately shifted sinebell function, necessarily decreases sensivity; weighting optimized for best sensitivity, e.g., with an exponential or a 90° shifted sinebell window function, necessarily yields nonattractive lineshapes with wide wings in the magnitude mode spectrum for this type of experiments.

Since even small coupling interactions are of interest, highest sensitivity, rather than optimized lineshapes, are of prime importance with $^nJ_{CH}$ correlation experiments. In order to compare the results on this basis, data processing was adjusted individually to obtain the highest sensitivity with each of the investigated experiments. Consequently, for the reasons given before, different lineshapes must be expected. Despite magnitude calculation, rather sharp lineshapes in the proton dimension F2 are obtained with the HMBC and the HMSC experiment, whereas less attractive resonance signals with wide wings are measured with refocused experiments such as the ACCORD-HMBC experiment (Fig. 3).

Experiments with a refocused HMSC variant with two additional BIRD elements prior to detection, allowing ^{13}C GARP broadband decoupling to be performed, have also been carried out. Increased intensities could be measured for only a few and usually for the most intense signals in the $^nJ_{CH}$ subspectrum, whereas for others even reduced intensities have been observed in the worst case. If the condition $D3 = (4 \cdot {}^nJ_{CH})^{-1}$ is violated, an unfavorable cumulative effect occurs on account of the additional delays, giving rise to a general decrease in sensitivity and a pronounced discrimination of weak vs intense cross peaks. The sensitivity is furthermore decreased by relaxation losses with this prolonged variant.

$^1J_{CH}$ subspectra are simplified due to signal collapse, however, and in contrast to the basic (refocused) HMQC experiment, only small—if any—sensitivity gains could be observed.

Modifications as recently proposed for the HMBC experiment, such as a constant time $t1$ evolution period for suppressing line broadening in the F1 dimension caused by homonuclear J-modulation (*7*) or the ACCORDION principle for systematically sampling $^nJ_{CH}$ couplings in a potentially wide range (*11, 13–15*), may easily be accomplished with HMSC.

CONCLUSION

Information on both long-range and one-bond coupling networks, deduced from correspondingly edited correlation spectra with the highest discrimination factors, are not only highly desirable for unequivocal signal assignments, but also a prerequisite for the reliable solution of more demanding structural problems.

We propose a new HMBC-derived 2D pulse sequence for the efficient measurement of $^nJ_{CH}$ and $^1J_{CH}$ connectivities taking advantage of a strategy which deviates considerably from the usual strategies in pulse sequence design. Instead of destructively suppressing "unwanted" $^1J_{CH}$ responses in the HMBC experiment by one or several filters, both types of coherences are detected simultaneously in each scan and in such a way that $^nJ_{CH}$ and $^1J_{CH}$ responses can be disentangled and corresponding connectivity maps can be calculated.

Despite similar sensitivities for the HMSC and the standard HMBC experiment for detecting $^nJ_{CH}$ interactions, and a less attractive sensitivity for the detection of $^1J_{CH}$ interactions, we find an overall gain in sensitivity results compared to the usual strategy with two $^1J_{CH}$ and $^nJ_{CH}$ dedicated experiments performed one after the other.

Features such as the outstanding suppression degree for $^1J_{CH}$ signals in the $^nJ_{CH}$ spectra for the whole range of one-bond and long-range couplings, the insensitivity to incorrectly set ^{13}C pulse angles, and the easy experimental setup with simple data processing make HMSC a valuable alternative to today's less-efficient two-experiment approach and suitable for routine applications.

ACKNOWLEDGMENTS

We gratefully acknowledge the financial support of the Swiss National Science Foundation. We thank Dr. P. Tregenna-Piggott, Department of Chemistry, University of Berne, for helpful advice and for proofreading the manuscript.

REFERENCES

1. A. Bax and M. F. Summers, ^{1}H and ^{13}C assignments from sensitivity-enhanced detection of heteronuclear multiple-bond connectivity by 2D multiple quantum NMR, *J. Am. Chem. Soc.* **108,** 2093–2094 (1986).
2. W. Willker, D. Leibfritz, R. Kerssebaum, and R. Bermel, Gradient selection in inverse heteronuclear correlation spectroscopy, *Magn. Reson. Chem.* **31,** 287–292 (1993).
3. S. Braun, H.-O. Kalinowski, and S. Berger, "150 and More Basic NMR Experiments," Wiley-VCH, Weinheim, 1998.

4. K. Furihata and H. Seto, Decoupled HMBC (D-HMBC), an improved technique of HMBC, *Tetrahedron Lett.* **36,** 2817–2820 (1995).
5. R. Marek, L. Králík, and V. Sklenár, Gradient enhanced HSQC experiments for phase-sensitive detection of multiple bond interactions, *Tetrahedron Lett.* **38,** 665–668 (1997).
6. S. Sheng and H. van Halbeek, Accurate and precise measurement of heteronuclear long-range couplings by a gradient enhanced two-dimensional multiple-bond correlation experiment, *J. Magn. Reson.* **130,** 296–299 (1998).
7. K. Furihata and H. Seto, Constant time HMBC (CT-HMBC), a new HMBC technique useful for improving separation of cross peaks, *Tetrahedron Lett.* **39,** 7337–7340 (1998).
8. G. Martin and A. Zektzer, Phase sensitive HMBC with BIRD filter, *in* "2D NMR Methods for Establishing Molecular Connectivity," pp. 267–273, VCH, Weinheim, 1988.
9. T. Parella, F. Sanchez-Ferrando, and A. Virgili, Purge scheme for efficient suppression of direct responses in gradient-enhanced HMBC spectra; *J. Magn. Reson. A* **112,** 241–245 (1995).
10. K. Furihata and H. Seto, 3D-HMBC, a new NMR technique useful for structural studies of complicated molecules, *Tetrahedron Lett.* **37,** 8901–8904 (1996).
11. R. Wagner and S. Berger, Accord-HMBC: A superior technique for structural elucidation, *Magn. Reson. Chem.* **36,** 44–46 (1998).
12. G. Bodenhausen and R. R. Ernst, Direct determination of rate constants of slow dynamic processes by two-dimensional "accordion" spectroscopy in nuclear magnetic resonance, *J. Am. Chem. Soc.* **104,** 1304–1309 (1982).
13. G. E. Martin, C. E. Hadden, R. C. Crouch, and V. V. Krishnamurthy, Accord-HMBC: Advantages and disadvantages of static versus accordion excitation, *Magn. Reson. Chem.* **37,** 517–528 (1999).
14. C. E. Hadden, G. E. Martin, and V. V. Krishnamurthy, Improved performance accordion heteronuclear multiple-bond correlation spectroscopy-IMPEACH-MBC, *J. Magn. Reson.* **140,** 274–280 (1999).
15. C. E. Hadden, G. E. Martin, and V. V. Krishnamurthy, Constant time inverse-detection gradient accordion rescaled heteronuclear multiple bond correlation spectroscopy: CIGAR-HMBC, *Magn. Reson. Chem.* **38,** 143–147 (2000).
16. NMRSIM (Bruker Analytik GmbH), Version 2.7 (1998).
17. J. R. Garbow, D. P. Weitekamp, and A. Pines, Bilinear rotation decoupling of homonuclear scalar interactions, *Chem. Phys. Lett.* **93,** 504–509 (1982).
18. M. H. Levitt, Composite pulses, *Progr. NMR Spectrosc.* **18,** 61–122 (1985).